Two-dimensional magnetohydrodynamic simulations of poloidal flows in tokamaks and MHD pedestal

L. Guazzotto[1,a)] and R. Betti[1,2]
[1]*Department of Mechanical Engineering, University of Rochester, Rochester, New York 14627, USA*
[2]*Princeton Plasma Physics Laboratory, Princeton, New Jersey 08540, USA*

(Received 11 June 2011; accepted 23 August 2011; published online 30 September 2011)

Poloidal rotation is routinely observed in present-day tokamak experiments, in particular near the plasma edge and in the high-confinement mode of operation. According to the magnetohydrodynamic (MHD) equilibrium theory [R. Betti and J. P. Freidberg, Phys. Plasmas **7**, 2439 (2000)], radial discontinuities form when the poloidal velocity exceeds the poloidal sound speed (or rather, more correctly, the poloidal magneto-slow speed). Two-dimensional compressible magnetohydrodynamic simulations show that the transonic discontinuities develop on a time scale of a plasma poloidal revolution to form an edge density pedestal and a localized velocity shear layer at the pedestal location. While such an MHD pedestal surrounds the entire core, the outboard side of the pedestal is driven by the transonic discontinuity while the inboard side is caused by a poloidal redistribution of the mass. The MHD simulations use a smooth momentum source to drive the poloidal flow. Soon after the flow exceeds the poloidal sound speed, the density pedestal and the velocity shear layer form and persist into a quasi steady state. These results may be relevant to the L-H transition, the early stages of the pedestal and edge transport barrier formation. © *2011 American Institute of Physics*.
[doi:10.1063/1.3640809]

I. INTRODUCTION

Reducing energy transport is crucial to the success of future devices in producing net power through thermonuclear fusion reactions with machines based on the magnetic confinement approach. Simply phrased, the inner region of the plasma must be kept sufficiently dense and sufficiently hot for a sufficiently long time in order to achieve a burning plasma state.[1] This is facilitated by the development of an edge transport barrier suppressing the heat losses out of the plasma. The problem is at least in part addressed by the existence of a high-confinement regime in tokamaks, commonly known as H-mode (as opposed to the low-confinement regime, the L-mode).[2] The lower energy transport in H-mode plasmas is explained by the presence of highly sheared edge flows inhibiting turbulent transport near the edge. H-mode plasmas feature steep density and temperature gradients near the plasma edge. Even though the transition between the two confinement regimes (L-H transition) is observed routinely and known to occur spontaneously when the input heating power is sufficiently high, no conclusive explanation has been provided to date.

On the theory side, the existence of magnetohydrodynamic (MHD) equilibria with "transonic" poloidal flows has been known for some time.[3–7] Transonic equilibria are characterized by strong shear (in the ideal case, discontinuities) in poloidal velocities and by density discontinuities at the same magnetic surface where velocity discontinuities are located. It has not been determined whether transonic equilibria are present in experiments, and whether they are related to the energy transport reduction that is observed in experiments. Nevertheless, some similarities are found between transonic equilibria and H-mode plasmas, the most crucial of which is the presence of highly sheared poloidal flows and edge pedestals.

In the present work, we will argue the hypothesis that transonic equilibria are related to H-mode plasmas, or more precisely, to the L-H transition.[8] The hypothesis is that if the poloidal velocity becomes supersonic, then a transonic equilibrium will automatically form, with a density pedestal and a high velocity shear in correspondence to the density pedestal. Temperature pedestals are formed depending on the value of the adiabatic index γ. Transonic flows do not produce temperature pedestals in isothermal plasmas $\gamma = 1$. However, since the energy transport across the transonic surface is greatly reduced in transonic equilibria with respect to static equilibria, it is expected that the reduction in radial energy transport will make the plasma temperature increase in the plasma core leading to an edge temperature pedestal. In this picture, the velocity shear and density pedestal will form first, on the fast time scales of magnetohydrodynamics. The temperature pedestal will form later on the slower transport time scales. In this work, numerical simulations are presented, which focus on the first part of the transition, and show how a subsonic equilibrium naturally develops discontinuous profiles where a supersonic poloidal flow is driven at the edge.

We remark for the sake of completeness that so-called "transonic" equilibria have in fact velocities that extend across the poloidal component of the slow magnetosonic velocity, rather than across a "sonic" speed, as the name suggests. The magnetoslow velocity is numerically almost identical to the sound speed in the systems under consideration in this work, and the slow magnetosonic wave is often (improperly) simply called "sound wave" in tokamak literature. However, the two are quite different, since the magnetoslow

a)Author to whom correspondence should be addressed. Electronic mail: luca.guazzotto@rochester.edu.

wave travels in the direction of the magnetic field, while sound waves have no preferential direction of propagation. We will conform to the standard nomenclature in the remainder of our paper, but the distinction just outlined should be kept in mind.

II. THE PHYSICAL PICTURE

The idea behind the existence of discontinuous transonic equilibria in the frame of ideal MHD has been addressed elsewhere,[3] and is only briefly reviewed here. In the simplest case of a low-beta (where $\beta = 2p/B^2$ is the ratio between plasma pressure p and magnetic pressure and B is the magnetic field), high aspect ratio plasma with circular cross section, the fundamental argument behind the existence of discontinuities in transonic equilibria is geometric (Fig. 1).

The shaded area in the top part of Fig. 1 represents the cross section for poloidal flow. If one assumes that the distance Δx between the two magnetic surfaces is constant along the cross section (as is reasonable for a circular, low-beta, high-aspect ratio tokamak plasma), the cross section for the poloidal flow is simply $2\pi\Delta x(R_0 + r\cos\theta)$, where θ is the poloidal angle measured from the outboard side of the plasma. Therefore, the cross section has a minimum at $\theta = \pi$ and a maximum at $\theta = 0, 2\pi$, and for all practical purposes is a De Laval nozzle for the poloidal flow, as shown schematically in the lower section of Fig. 1. From one-dimensional ideal gasdynamics for isentropic flows (neglecting for the time being the effect of the flow on the magnetic field), it is known that a subsonic flow will accelerate (increase its Mach number) along the poloidal angle between 0 and π, while a supersonic flow will decelerate (decrease its Mach number), as shown in Figs. 2(a) and 2(b). Velocity and Mach numbers are symmetric with respect to $\theta = \pi$, if the flow does not change its characteristic (either subsonic or supersonic) during a poloidal revolution. Transition from the subsonic to the supersonic regime along the flow are obtained in De Laval nozzles when the Mach number is less than one from the inlet to throat, exactly equal to one at the throat and larger than one from the throat to the outlet. However, the traditional subsonic-to-supersonic flow that develops in De Laval nozzles cannot occur at steady state in a periodic system, since the velocity at $\theta = 2\pi$ (supersonic in the accelerating nozzle) must be equal to the velocity at $\theta = 0$ (subsonic in the accelerating nozzle). If a subsonic-to-supersonic transition occurs, the velocity must come back to subsonic values because of periodicity. In an ideal system, this can only occur in the presence of a shock. Since shocks are dissipative, entropy-generating phenomena, they cannot exist at steady state, since they would require a powerful mechanism for exhausting the large entropy production. Therefore, on each magnetic surface the flow can only be either subsonic or supersonic. The Mach number varies on the magnetic surface as described before, reaching a maximum value (at most $M_p = 1$) at $\theta = \pi$ for subsonic flows (Fig. 2(a)), and a minimum value (no less than $M_p = 1$) at $\theta = \pi$ for supersonic flows (Fig. 2(b)). We then conclude that any value for M_p is allowed at $\theta = \pi$, but that anywhere else in the plasma there will be a range of prohibited Mach numbers, with the range of prohibited numbers increasing the farther one moves from $\theta = \pi$, as shown in Fig. 2(c). The Mach number *radial* discontinuity at all angular locations except $\theta = \pi$ is what is called *transonic discontinuity* in this work. The discontinuity

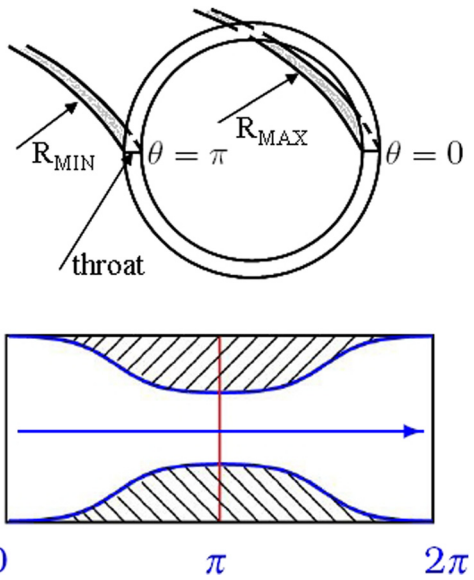

FIG. 1. (Color online) Top: Schematic representation of the variation of the cross section for poloidal flow (shaded area) due to toroidal geometry. Bottom: Cross section for poloidal flow (indicated by the arrow) as a function of poloidal angle. The outer midplane corresponds to $\theta = 0$.

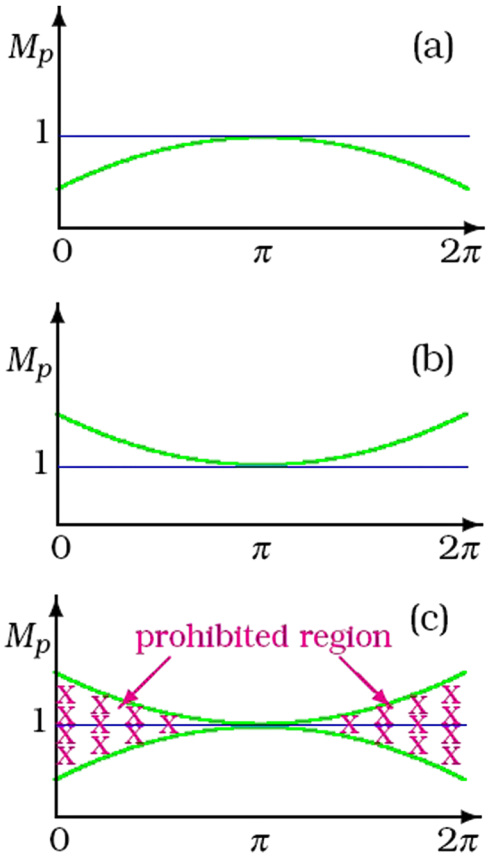

FIG. 2. (Color online) Mach number profiles for subsonic (a) and supersonic (b) flows. The shockless transonic equilibrium situation is shown in (c). In (c), the two curves correspond to the Mach number profiles on the two sides of the transonic discontinuity.

in Mach number will also cause a discontinuity in density, pressure, and velocity; density discontinuity in particular is referred to as the *transonic pedestal* in the remainder of this work. In this gasdynamic picture, the relevant speed for the present argument is the poloidal sound speed $C_{sp} \equiv C_s B_p/B$, where B_p is the poloidal component of the field and C_s the sound speed. The Mach number introduced earlier in the discussion is thus defined as $M_p \equiv V_p/C_{sp}$, where V_p is the poloidal velocity.

In standard tokamaks $B_p \ll B$ and, therefore, $C_{sp} \ll C_s$, numerical values for C_{sp} are given later in the paper. Since $B_p = 0$ on the magnetic axis and the plasma temperature is small at the edge, the poloidal sound speed has a profile similar to the one shown in Fig. 3 (blue curve). Based on the previous discussion, the only poloidal velocity profile allowed at equilibrium is the discontinuous one qualitatively represented by the red curve in Fig. 3. A continuous profile like the one represented by the dotted line is not allowed at steady state. It is very important to emphasize that the discontinuity is a tangential discontinuity, occurring between two streams flowing next to each other, without any flow across the discontinuity. We speculate that the velocity discontinuity (i.e., strong sheared flow) cause a transport barrier[9] leading to improved energy confinement regimes

Before proceeding with our analysis, it is useful to emphasize the relation between the one-dimensional gasdynamic picture and a real plasma. In our description, we observed that the plasma is forced to flow between magnetic surfaces, i.e., along magnetic field lines. In the limit of $\beta \to 0$, the plasma does not affect the magnetic field, which behaves as a rigid wall. Thus, the characteristic speed that separates sub- and super-sonic flows is a velocity with the magnitude of the sound speed and the direction of the magnetic field. If β is finite, the plasma flow will also affect the magnetic field, in a way that is determined by energy conservation along the field lines.[10] We then conclude that for finite betas the characteristic velocity to be taken into account is a velocity that travels along the field lines, and has a magnitude that depends on plasma pressure and magnetic field strength, and reduces to the sound speed for vanishing β. We immediately recognize this to be the slow magnetosonic velocity. Therefore, sub- and super-"sonic" flows should more correctly called sub- and super-"magnetoslow" flows. For ease of notation and following the literature, we will keep the "sonic" terminology in the remainder of the paper, but the physical sense of the distinction must not be forgotten. Moreover, the poloidal "sound" speed C_{sp} should more correctly be defined as poloidal "magnetoslow" speed, i.e., $C_{sp} \equiv A_s$, with

$$A_s = \sqrt{\frac{\gamma p + B^2 - \sqrt{(\gamma p + B^2)^2 - 4\gamma p B_p^2}}{2B_p^2}}\frac{B_p}{\sqrt{\rho}} \simeq \sqrt{\frac{\gamma p}{\rho}\frac{B_p^2}{\gamma p + B^2}}. \quad (1)$$

The approximate expression holds for low beta, and it is easy to realize that for $\beta \to 0$ A_s reduces to the poloidal sound speed defined above. (Of course our discussion is only a brief intuitive description of the issue at hand. For a proper treatment of waves in plasmas, see e.g., Refs. 11 and 12). In the remainder of this paper, we will use the definition of C_{sp} given by Eq. (1), but for ease of representation we will at times approximate its numerical value with $C_{sp} = A_s \simeq (\sqrt{\gamma p/\rho})(B_p/B)$. Since in the region where the transonic pedestal forms $\beta \ll 1$ (typically, $\beta \sim 10^{-3}$), the numerical error due to this approximation is negligible.

After examining transonic equilibria, the natural question arises of what will happen if an initial continuous transonic velocity profile is assigned to a time-evolving system, or equivalently, if a (sufficiently large) smooth poloidal velocity source is inserted in a static system. We will consider the more meaningful case of a smooth velocity source. As the source deposits poloidal momentum in the system, the plasma will spin up, with velocity increasing in time but with a (radially) continuous profile everywhere in the plasma. At some point, the velocity will become supersonic (with respect to C_{sp}). For simplicity, we can ignore further effects of the momentum source. Since the velocity, pressure, and density profiles are continuous, the Mach number profile is also continuous and, therefore, there is a region in the plasma where the Mach number falls in the forbidden range. A soon as the plasma "knows" about the periodicity of the system, it will evolve the velocity profile in order to satisfy the periodic boundary condition. In the case of a strong source, as mentioned earlier, this will result in the formation of a shock. The shock travels in the poloidal direction along the flow, until it reaches the inner part of the cross section (i.e., the nozzle throat). The shock disappears at the throat, leaving a system at steady state. It is very important to stress that the MHD pedestal is **not** created by the shock. What the shock does is rearrange the velocity profile in such a way that there is no plasma flowing in the prohibited regime, but the density discontinuous profile is determined by MHD force balance at equilibrium. Therefore, even though the shock may not occur in experiments due to the long particle mean-free path, we speculate that the final discontinuous shockless steady state is correct, since it is the only equilibrium solution allowed by MHD.

An important new finding of this work with respect to transonic equilibrium calculations is the effect of mass redistribution during the transient. As the velocity profile evolves to form a discontinuity between the subsonic and the

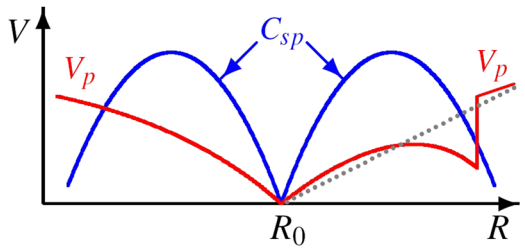

FIG. 3. (Color online) Sketch of poloidal velocity (red, V_p label) and poloidal sound speed (blue, C_{sp} label). The profile represented with a dotted line is not allowed at steady state by MHD force balance. The discontinuous solid line is the only possible transonic solution. R_0 is the magnetic/geometric axis (Shafranov shift is neglected in the sketch).

supersonic region peaked on the outboard side, the density profile also evolves to a steady-state satisfying mass and energy conservation. The supersonic root of the equilibrium has a density that is lower than the corresponding subsonic root.[3,4,10] For that reason, and since the initial condition for the formation of the transonic pedestal is a static (or subsonic) plasma, mass needs to be removed from the supersonic region. In ideal MHD, this cannot happen with radial mass transport. The only way to redistribute the plasma mass is to transport mass in the poloidal direction to the region where there are no constraints on the density and Mach number profiles, i.e., to the inboard section of the plasma. The mass accumulation in the inboard section of the plasma also creates a pedestal, which is not across a transonic discontinuity, but only due to mass conservation. In order to distinguish this pedestal from the transonic pedestal, we name it the *inner pedestal*, and refer to the resulting pedestal at all angular locations as to the *MHD pedestal*. The inner pedestal is also found in transonic equilibrium calculations, but only if some special choice is made for the input profiles, which only becomes natural if one keeps into account the properties of the corresponding static equilibrium.

As pointed out by McClements and Hole,[13] it is unlikely that current tokamak plasmas rotate poloidally at supersonic velocity in the core region. For a high performance H-mode plasma the central temperature reaches several kiloelectron volts and the poloidal sound speed exceeds 100 km/s. Therefore, if the transonic discontinuity plays any role at all in current experiments, its effects are likely restricted to the plasma edge, the edge pedestal, and the edge transport barrier, where supersonic flows require poloidal velocities of tens of km/s.

The purpose of the present work is to confirm the predictions of theory with time-dependent simulations showing the formation of transonic discontinuities and MHD pedestal starting from a static equilibrium.

III. PLASMA DESCRIPTION

A. Theoretical model

The present work is based on the standard single-fluid MHD description of the plasma. The physical model described in Sec. II only requires the basic ideal-MHD equations. By the discussion in Sec. II is also clear that the mechanism for the MHD pedestal formation is a two-dimensional toroidal effect requiring to solve the system evolution in time and two spatial dimensions. Moreover, the analysis in Ref. 3 assumes a circular cross section for a high aspect ratio and low-beta plasma. Those simplifications are useful for obtaining an intuitive picture of the MHD pedestal formation, but are not necessary in the present work. Indeed, it is easily verified with equilibrium calculations that discontinuous transonic equilibria are valid solutions in toroidal plasmas, regardless of β, plasma shape, and aspect ratio. Therefore, a model allowing for arbitrary plasma properties is used in this work. An additional element that is included in the analysis is the presence of a "vacuum" region outside the plasma. This is done for a number of reasons. First, we want to include X-points close to the plasma in our numerical simulations, in order to study realistic tokamak configurations. Next, we want to confirm that the transient bringing to the formation of the MHD pedestal does in fact leave the plasma mostly unperturbed. That is verified by leaving the plasma free to move in a free-boundary simulation and by observing that it does not shift its position in any meaningful measure. In addition to this, there are numerical reasons that make a free-boundary simulation easier to handle from the point of view of boundary condition implementation, as is discussed in Sec. III 2.

Based on the previous discussion, the system is described with the time-dependent, two-dimensional set of resistive MHD equations,

$$\frac{\partial \rho}{\partial t} + \nabla \cdot (\rho \underline{V}) = 0, \tag{2}$$

$$\frac{\partial \rho \underline{V}}{\partial t} + \nabla \cdot \left(\rho \underline{V}\underline{V} - \underline{B}\underline{B} + P\underline{\underline{I}} \right) = \underline{S}_{mom}, \tag{3}$$

$$\frac{\partial \underline{B}}{\partial t} = \nabla \times (\underline{V} \times \underline{B} - \eta \underline{J}), \tag{4}$$

$$\frac{\partial \mathcal{E}}{\partial t} + \nabla \cdot [(\mathcal{E} + P)\underline{V} - \underline{B}(\underline{V} \cdot \underline{B}) + \eta \underline{J} \times \underline{B}] = \underline{V} \cdot \underline{S}_{mom}, \tag{5}$$

where $\underline{B}$ is the magnetic field, $\underline{V}$ the plasma velocity, ρ the density, $\underline{J}$ the current, $P \equiv p + \frac{B^2}{2}$ the total pressure, $\mathcal{E} = \frac{p}{\gamma - 1} + \rho \frac{V^2}{2} + \frac{B^2}{2}$ the total energy, γ the adiabatic index, η the resistivity. Here and in the remainder of this paper, we have set $\mu_0 = 1$ for ease of notation. The term S_{mom} on the right-hand side of Eqs. (3) and (5) corresponds to the momentum source that is used to drive the plasma poloidal rotation and is discussed in Sec. IV. Equations (2)–(5) are (in that order) the standard resistive-MHD equations for mass conservation, momentum conservation, Faraday's law (complemented by Ohm's law), and energy conservation. For reasons that will be described shortly, Eqs. (2)–(5) are written in conservative form.

We observe that a definition of η is necessary to complete the system (2)–(5). In principle, one could assign a very small resistivity value in the main plasma region and a very high value in the "vacuum" region, thus modeling an effective vacuum as a highly resistive plasma. Alternatively, it is possible to model the "vacuum" region as a low-temperature, low-density plasma. This is easily accomplished by defining the resistivity through Spitzer's formula, $\eta \sim T^{-3/2}$, where T is the plasma temperature. In either case, an evolution equation for the resistivity is needed, since the evolution of the resistivity profile corresponds to the evolution of the plasma-vacuum interface. For the simulations presented in the remainder of this work, the second choice was made. The "vacuum" region is therefore more correctly referred to as a "halo" region. The resistivity profile is then evolved through the temperature, which is self-consistently calculated from the pressure and density profiles. For completeness, it is mentioned that simulations with higher resistivity for the vacuum region were also performed, and that the resistivity profile has a negligible effect on the main part of the transient, i.e., the evolution of the plasma properties in the region with closed field lines.

B. Numerical implementation

In this section, we describe the MHD simulation code SIM2D,[8] which was developed to study the evolution of poloidal flows and the formation of MHD pedestals. Based on the discussion in Sec. II, the numerical solution of the system of equations (2)–(5) needs to be suited for first correctly reproducing the shock evolution during the transient phase and second preserving discontinuities in the shockless steady-state phase of the simulations. The first requirement is most naturally satisfied by using any of the standard shock-capturing methods. As for the second one, a non-diffusive scheme is preferable, since numerical diffusion would smear out the tangential discontinuities in the pedestal, and artificially prevent the simulations from creating long-lasting discontinuous profiles for all relevant plasma properties. It is also necessary to observe that the model in Eqs. (2)–(5) does not include any dissipation (other than resistivity and numerical viscosity) and will, therefore, only evolve to a true steady state slowly, due to the small numerical viscosity. As detailed in the next section, the final state of the simulations is instead a shock-free quasi steady state, in which the plasma properties are still slowly evolving in the poloidal direction, but radial discontinuities are present.

The requirements just highlighted directed us to choose a scheme based on the conservative-form system of evolution equations, which automatically satisfy the shock-capturing requirement. We then picked the relatively simple finite-difference predictor-corrector MacCormack scheme,[14] which is second-order accurate in both space and time, and which is not diffusive. The time-evolution scheme is explicit and conditionally stable, requiring to satisfy the standard Courant–Friedrichs–Lewy condition. Our choice of time-stepping method makes it necessary to include artificial dissipation in the system. That is because the method is dispersive, even though it is not diffusive. Dispersive errors can cause problems (i.e., Gibb's effects) in high-gradient regions and are, therefore, controlled by numerical diffusion. This is not in contrast with the requirement of having a non-diffusive solution of the time evolution of our system: Artificial diffusion is only turned on in the presence of unphysical spikes, which are automatically detected by the code. Small additional artificial terms (artificial viscosity and thermal conduction) are also introduced for numerical reasons, mostly to counteract the effects of the misalignment between the (Cartesian) grid and the "natural" direction of the evolution of the system (i.e., the poloidal magnetic field direction).

An additional difficulty is due to the fact that the "diffusive" part of Eq. (4), i.e., the part of the evolution equation for the magnetic field that is due to the presence of a finite resistivity, is not well-suited for an explicit solution like the one just described. The problem is solved by splitting Eq. (4) in two parts,

$$\frac{\partial \underline{B}}{\partial t} = \nabla \times (\underline{V} \times \underline{B}), \tag{6a}$$

$$\frac{\partial \underline{B}}{\partial t} = -\nabla \times (\eta \underline{J}). \tag{6b}$$

Equation (6a) is advanced using the predictor-corrector algorithm, while Eq. (6b) is advanced using an alternate-direction implicit (ADI) method. The ADI method requires the solution of a series $(3 \times (N_R + N_Z)$, where N_R, N_Z are the number of points in the R and Z directions) of tridiagonal systems at each time step. The systems are tridiagonal due to direction splitting; for the same reason, the dimension of each system is only equal to the number of points in either direction. Therefore, the solution of Eq. (6b) does not need a large computational time compared to the solution of the rest of system (2)–(5).

It is well-known that a time-advancement scheme for the magnetic field like the one just described does not automatically conserve the divergence-free property $(\nabla \cdot \underline{B} = 0)$ of the field, regardless of the accuracy of the initial conditions.[15] It is also known that allowing the error $\nabla \cdot \underline{B} \neq 0$ to grow in time has catastrophic effects on the stability of the numerical method. Therefore, it is necessary to correct the divergence error. This is accomplished by using a standard projection method,

$$\begin{aligned} &\nabla \cdot \underline{B}^{(n,*)} \equiv \Lambda \neq 0, \\ &\underline{B}^{(n)} \equiv \underline{B}^{(n,*)} + \nabla \Phi, \\ &\nabla \cdot \underline{B}^{(n)} \equiv 0 \rightarrow \nabla^2 \Phi = -\Lambda, \end{aligned} \tag{7}$$

where $\underline{B}^{(n,*)}$ is the magnetic field at the *nth* time step before divergence correction, $\underline{B}^{(n)}$ the magnetic field at the *nth* time step after divergence correction, $\Phi(R, Z)$ is an auxiliary scalar potential, and Eq. (7) is solved for Φ with a standard Successive-Over-Relaxation method at each time step.

Initial conditions for the simulations are assigned from a numerical equilibrium calculation. The preferred approach is to use an equilibrium calculated with the code FLOW,[4] but in principle any numerical equilibrium can be used as a starting point for the simulations. One advantage of the FLOW code is the possibility of having a rotating equilibrium as initial condition. Moreover, FLOW has been extended to calculate free-boundary equilibria, thus allowing for arbitrary geometry and realistic plasma conditions to be used as initial condition for SIM2D simulations. More details on the initial conditions used for the simulations presented in this work are contained in Sec. IV.

The final point that needs to be addressed in the present section is the implementation of boundary conditions. In a fixed-boundary simulation, ideal-wall boundary conditions can be used. In this case, the normal components of the plasma velocity and the magnetic field are set to zero, while the tangential components are set to be continuous. In the case of free-boundary simulations, the computational boundary is assumed to correspond to the first wall of the tokamak, which on the time scale of MHD can be considered to be a superconductive wall. However, this does not mean that the normal velocity and magnetic field must vanish on the wall. On the contrary, the initial magnetic field enters into the wall. This is shown in Fig. 4, in which magnetic surfaces are plotted with black lines. Since magnetic surfaces intersect the computational boundary (i.e., the wall), the poloidal field, tangential to magnetic surfaces, also intersects the

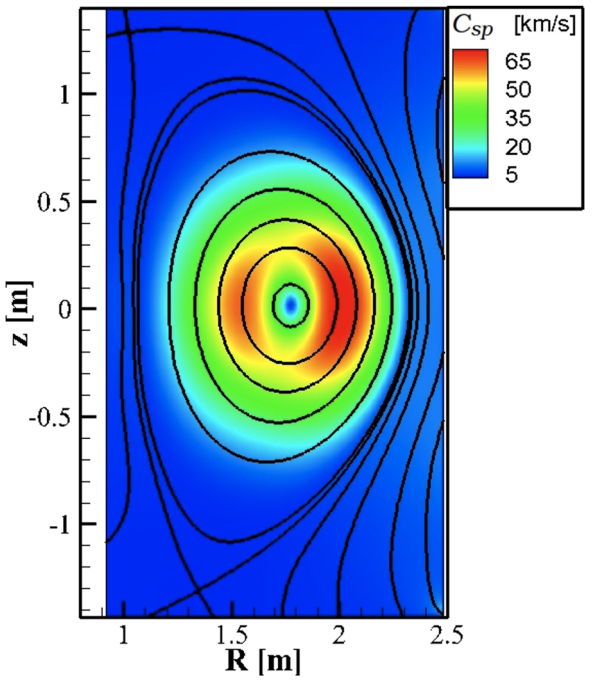

FIG. 4. (Color online) Poloidal sound speed [km/s] (colormap) and magnetic surfaces (lines). The first plotted magnetic surface inside the LCFS is assigned as plasma edge.

wall. The superconductive wall assumption corresponds to keeping the magnetic field on the wall constant. As for the plasma velocity, plasma is free to flow along field lines at the thermal velocity. In our simulations, we use the condition,

$$\underline{V}_{boundary} = \alpha_{boundary} C_s \frac{\underline{B}}{|B|} \operatorname{sign}(\underline{B} \cdot \hat{n}), \tag{8}$$

whit $\alpha_{boundary} \leq 1$. Values $\alpha_{boundary} < 1$ are used in our simulations to avoid resolving the sheath next to the plasma wall (velocity is subsonic away from the wall, and only gets to the sonic speed close to the wall). Equation (8) defines the velocity to be into the wall regardless of the sign of the magnetic field ($\hat{n}$ is the outward-directed unit vector normal to the wall). In order to avoid having too large mass variations during the transient, a self-adjusting recycling routine is added to the code. The recycling algorithm adds a uniform (in space) source term to the continuity equation in the "halo" region. At each time step the total mass in the halo region is compared to the initial mass; if the mass is smaller than the initial mass the source term is increased, if it is larger the source term is decreased. Even though rather crude in terms of plasma-wall interaction physics, the set of boundary conditions and recycling just described is sufficient for the purpose of our simulations. It is stressed that the main focus of the work is in the evolution of the main plasma region, while the "halo" region serves the sole purpose of allowing a self-consistent evolution of the shape of the plasma-vacuum boundary.

It is worthwhile to observe at this point that numerical time-dependent simulations will generate equilibrium profiles with sharp gradients instead of the exact discontinuities predicted by ideal MHD. This is partly due to numerical reasons (e.g., resolution, numerical dissipation), and partly to the fact that there is physical dissipation in the system, due to the finite resistivity used in the simulations.

To conclude the present section, a few details on the numerical simulations are included. Since the purpose of our simulations is to resolve the sharp gradients at the MHD pedestal, spatial resolution is a critical element in the simulation setup. Moreover, it is desirable to have a finite number of points in the halo region, making low-resolution runs incapable of resolving the halo region. In general, simulations with less than 200 points in each direction are too poorly resolved to be useful; but in practice, a resolution of at least 300 points is preferred. Resolutions up to 500 points in each direction are used in the results presented in the present work. It is also pointed out that since the dissipation present in the system is only numerical/artificial, it strongly depends on the grid steps. Therefore, different resolutions require different source levels to reproduce the same transient. This was verified with convergence studies. Moreover, if N is the number of points in each direction, the computational load is proportional to N^2, while the time step depends on $1/N$. Therefore, the computational time scales roughly with N^3. Regarding computational (wall) time, some improvements are obtained with a parallel version of SIM2D. For the time being, only some parts of the code have been parallelized, and the parallelization is handled via OPENMP. The code is ran on up to eight cores (on a single node). Preliminary testing shows that a more profound analysis is going to be necessary in order to take advantage of larger numbers of processors, as inter-processor communication already limits the speed gain when using four processors to about a factor of two.

IV. NUMERICAL SIMULATIONS

A. Simulation setup

In this section, we describe some numerical results obtained with the SIM2D code, which show the formation of a discontinuous transonic equilibrium starting from a static equilibrium and adding a continuous source for momentum generation. The intent of the present work is to show a proof of principle of the formation of discontinuities due to the presence of transonic poloidal flows, and not to model any specific experimental discharge.

For that reason, we use a baseline equilibrium (shown in Fig. 4) meant to reproduce some reasonable experimental parameters of the DIII-D tokamak, but we do not consider any specific discharge or equilibrium reconstruction as starting point for our simulations. The chosen model equilibrium is designed to reproduce the main properties of an L-mode plasma well before the L-H transition. Table I summarizes the relevant equilibrium properties. From Fig. 4 it is possible to recognize that the poloidal sound speed is low ($\lesssim 10\ km/s$) in a large part of the computational domain, and in particular at the edge of the main plasma region. In Fig. 4 the main-plasma edge corresponds to the first closed magnetic surface inward of the LCFS. For that reason, we expect from the beginning that transonic discontinuities will develop near the edge for velocities in the range of tens of km/s. This is also confirmed by equilibrium calculations.[16] Figure 4 also shows the presence of an X-point in the lower part of the

TABLE I. Main plasma parameters for the DIII-D model equilibrium.

Parameter	Meaning	Value
β_t	Toroidal beta $= 2\langle p\rangle/B_V^2$	1.12%
I_p	Plasma current	721 kA
β_p	Poloidal beta $= 2\langle p\rangle/\langle B_p\rangle^2$	0.42
R_0	Major radius	1.69 m
a	Minor radius	0.6 m
B_V	Vacuum field	1.26 T
T_E	Edge temperature	30 eV
T_C	Temperature on axis	3 keV

computational domain, and of a secondary X-point next to the top-left corner of the computational region. The initial condition corresponds to a lower-single-null (LSN) configuration.

Equations (2)–(5) contain the index γ. The choice $\gamma = 5/3$ corresponds to an adiabatic closure, while for $\gamma \to 1$ an isothermal closure is obtained. On the time scale of interest for our simulations, it is appropriate to assume isothermal flux surfaces, due to the rapid heat conduction parallel to the magnetic field, and therefore an isothermal closure. In the simulations, a value $\gamma = 1.05$ was used to approximately reproduce the isothermal closure within our formulation.

As shown in Eqs. (2)–(5), a momentum source S_{mom} is introduced in the system to drive the poloidal rotation. One important point in the discussion of the MHD pedestal formation is that *any* source that makes the poloidal velocity larger than the poloidal magneto-slow speed will result in the formation of an MHD pedestal. In this sense, our model does not depend on any specific mechanism for driving the flow. The study of poloidal momentum source is certainly an important topic, which is deferred to future times. For the proof-of-principle purpose of the present work, an arbitrary shape can be used for S_{mom}. However, it is intuitive that discontinuities will form if a *discontinuous* shape is chosen for S_{mom}. The purpose of the present work is to prove that discontinuities will also form if the source has a *continuous* (i.e., smooth) shape. Focusing in particular on the velocity profile, it is seen from Eq. (3) that in order to have a continuous source of velocity even if the density profile is discontinuous, the momentum source itself needs to be proportional to the plasma density. The shape of the velocity source and of the velocity after the formation of the MHD pedestal is shown in Sec. IV B (Fig. 8). In principle, even a constant (in space and time) source of velocity will generate transonic equilibria. However, a source that makes the poloidal velocity increase linearly in time will cause the transonic surface (the surface where $V_p = C_{sp}$) to move in time, which is an undesirable effect, since the intent is to observe the formation and permanence at (quasi) steady state of the MHD pedestal. Therefore, a source profile peaked at the edge is preferred for the simulations. Various strategies were considered, for instance a source dependence on the distance from the (initial or time-evolving) plasma edge, and dependence on the (initial) poloidal magnetic flux. If the distance from the edge is used, one must keep in mind that the distinction between halo and main-plasma regions is not well defined, so some consistent additional strategy needs to be devised to define the plasma-halo interface. Since simulations show that the plasma does not move appreciably during the transient, and in particular the magnetic field is essentially unperturbed by the transient, it is convenient to use the initial poloidal flux as a radial coordinate for the source strength. Finally, the source strength is also modulated in the poloidal angle. This is done to qualitatively reproduce a source due to non uniform phenomena, like for instance turbulence driven by unfavorable magnetic curvature in the outboard part of the plasma or ion-orbit losses. Based on the previous considerations, the following form was selected for the momentum source:

$$S_{mom} = \alpha\rho(\psi - \psi_m)^2 \cos\left(\frac{\theta}{2}\right) \quad \text{if } \psi > \psi_m, \qquad S_{mom} = 0 \quad \text{if } \psi < \psi_m, \tag{9}$$

where α is a dimensional input parameter that regulates the source strength, θ is the poloidal angle, ψ is the (initial) poloidal flux (normalized to be 0 on axis and maximum at the main plasma edge), and $\psi_m < \psi_{edge}$ is an input parameter. There is no source in the halo region.

Even though in the present work we will only present results obtained with the source shape given by Eq. (9), different shapes were tested with and without θ dependence and with and without density dependence. As long as the source is strong enough to drive transonic poloidal flows, the transient is qualitatively similar and the MHD pedestal will form. It is stressed once more that the only requirement for the formation of the MHD pedestal is the presence of transonic poloidal flow. The source shape and strength will only determine the quantitative details of the transient. In the present work, a relatively large source is used at the beginning of the transient, in order to quickly bring the edge flow to the supersonic regime and reduce the transient and simulation times. The source is reduced after the pedestal formation, to a level that either leaves the edge velocity approximately constant, or lets the edge velocity decrease slowly, in order to prove that the pedestal will survive as long as the edge flow is supersonic. Regarding source strength, very weak sources are sufficient to drive transonic flows. That is due to the absence of poloidal viscosity in our model. For the present work, it is assumed that the source is large enough to overcome poloidal viscosity and drive the flows obtained in our simulations. At any rate, we point out that poloidal viscosity is known to decrease for supersonic flows;[17] thus we do not expect that unreasonably large sources will be needed to drive transonic flows. A model of poloidal viscosity and a more quantitative evaluation of the power necessary to drive transonic flows and create MHD pedestals will be the object of future work. A simple estimate of the power dissipated by the poloidal viscosity is given in Sec. V.

B. Simulation results

In this section, we show some results of SIM2D numerical simulations. Unless otherwise noted, all plots are based on simulations with 500 grid points in each direction. Before discussing any result, it is useful to introduce a time scale for the system under consideration. We normalize all times to the

typical revolution time τ_p, which is defined as the time that a fluid element traveling at 40 km/s needs to complete a poloidal revolution at the plasma edge. The velocity of 40 km/s is chosen as a typical peak poloidal velocity at the end of the transient (as shown later). The revolution time τ_p only gives an order of magnitude for the time scale of the transient, since the poloidal velocity is a function of both time and position during the transient, with faster velocities developing at the beginning of the simulation. Since the plasma is not rotating as a rigid body, the supersonic region will complete a revolution in times shorter than τ_p (particularly at the beginning of the transient, when velocities are highest), while the subsonic region (which is not affected by the transient) will need times longer than τ_p. The fast initial rotation is partly due to the fact that a large source of poloidal momentum is used at the beginning of the simulation, with the purpose to shorten simulation times. Indeed, poloidal flow becomes supersonic in the outboard region of the plasma in a time $\sim 0.1\tau_p$.

Coming now to simulation results, theory predicts that a shock will form shortly after the flow becomes supersonic. The shock then travels poloidally in the direction of the flow until it reaches the nozzle throat. In our simulations, we chose to have relatively low velocities in the system, and therefore weak shocks. This makes the shock rather difficult to visualize in our numerical results. Since the focus of our work is not in the formation and evolution of the shock, but in the formation of the MHD pedestal, we do not invest any additional effort in analyzing the behavior of the shock. Before proceeding to discuss the properties of the MHD pedestal after the initial transient, it is stressed once more that a shock may not develop in the experiments due to the particle long mean free path. However, it is argued in the following that the formation of the pedestal does not depend on the shock, and thus it is expected that the final state should be realistic, even if part of the transient is not. For completeness, it is mentioned that the maximum poloidal velocity observed in the simulation corresponding to the results presented in this section is $V_{MAX} \simeq 88\,\mathrm{km/s}$. Such high velocity is only maintained for a short section of the transient. Moreover, MHD pedestal formation is observed also with slower maximum velocities, although at the price of longer transients and longer simulations. Once again, the discontinuous solution is the only equilibrium solution allowed by (ideal) MHD in the presence of transonic poloidal flows.

The presence of a pedestal structure is confirmed by the three-dimensional representation of simulation results shown in Fig. 5.

The pedestal structure after the shock disappearance is shown in the center pane (b) and compared on the left (a) with the initial condition of the simulation and on the right (c) with a transonic equilibrium calculated with FLOW[4] to approximately reproduce the plasma conditions of the simulations. Figure 5(b) shows that there is a clear steepening of the edge density profile, as compared with Fig. 5(a). The transonic pedestal structure is very well defined in the outboard side of the plasma, while the pedestal height decreases in the region closer to the inner side of the plasma. This is qualitatively consistent with the theoretical predictions of Ref. 3. Figure 5(b) also shows the presence of the inner pedestal, i.e., of the density pedestal in the inboard section of the plasma. The fundamental difference in character of the two pedestals (inner and transonic) is highlighted by the location of the sonic surface, represented with a black line in Fig. 5. The inner pedestal *is not* due to a jump in Mach number and is entirely located in the supersonic region, the transonic pedestal *is* due to a jump in Mach number, and extends across the $M_p = 1$ line. The combination of inner and transonic pedestal results in the creation of an MHD pedestal with a clear density sharp gradient at all poloidal locations. The shape of the MHD (inner + transonic) pedestal is reproduced in Fig. 5(c) with a transonic equilibrium calculation. In this case, input corresponding to a density profile peaked near the transonic surface was assigned, resulting in a density discontinuity across the $M_p = 1$ line in the outboard part of the plasma, and a steep gradient in the supersonic region in the inboard part of the plasma. To further clarify the qualitative difference between the two sharp-gradient regions, we remark that the transonic discontinuity in the equilibrium calculation occurs at a location where all input free functions are smooth, while the sharp gradient in the inboard side corresponds to a sharp gradient in one of the input functions. Figure 5(c) effectively proves that the MHD pedestal solution (with a pedestal at every angular location) is indeed an equilibrium solution. The difference in shape of the external

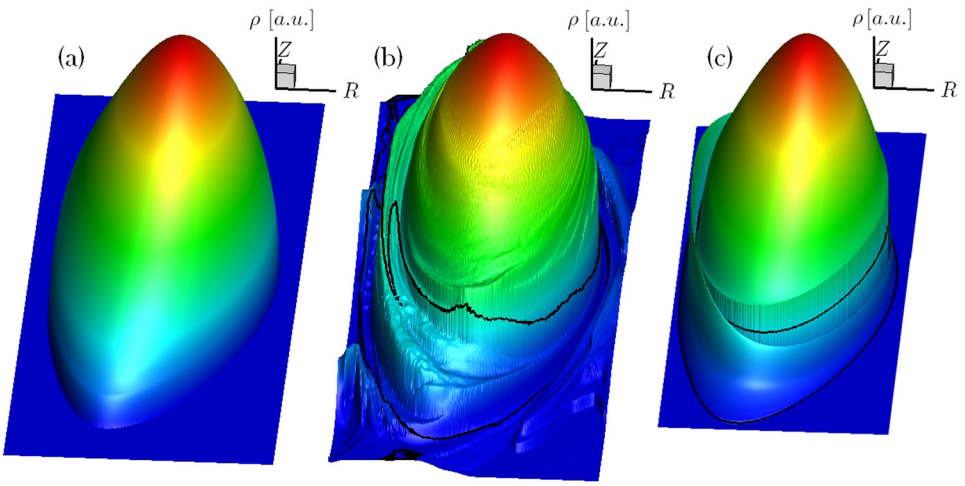

FIG. 5. (Color online) Plasma density at time $t = 0$ (a), at time $t = 2.5\tau_p$ (b), and for a transonic equilibrium (c). The black line indicates the surface $M_p = 1$.

boundary between Figures 5(b) and 5(c) is due to the fact that the "vacuum" region was not considered in the fixed-boundary equilibrium calculation, and a constant value was assigned for the density outside the plasma boundary (represented by the external black line in the figure). Thus, the "vacuum" region is meaningless in Fig. 5(c) and its size was therefore minimized. Figures 6 and 7 show a one-dimensional comparison between the equilibrium calculation and the SIM2D quasi-steady state (plots are at time $t = 2.1\tau_p$). The similarity between FLOW and SIM2D results is clearly visible. In particular, the two density profiles in Fig. 6 are very well matched in the pedestal region on both sides (transonic pedestal and inner pedestal). A clear difference is present inward of the inner pedestal. The difference does not have any profound meaning (it is located in the subsonic region) and is due to the choice of free-functions used for the FLOW equilibrium calculation. There is no direct approach to reconstruct FLOW free functions starting from SIM2D data, so the input for FLOW was determined by trial and error, with the main focus being on the sharp gradient regions, which are indeed well matched in the two solutions. Thus the profile difference in the inboard part of the plasma inward of the pedestal region is an effect of the imperfect match between the free functions and the SIM2D snapshot. One should also keep in mind that the cold edge region has finite resistivity in SIM2D, as compared to the ideal plasma model of FLOW. Moreover, in the edge region density and velocity are strongly modified with respect to the initial condition, and these modifications have not yet reached an exact steady state, i.e., an equilibrium. This also complicates the task to evaluate the input for FLOW in the edge region, where profiles on a magnetic surface are less smooth than in an equilibrium calculation. As shown later (Fig. 9), the height of the inner pedestal peak also varies in time. The height used in the FLOW input is an approximate average during the quasi-steady state phase of the time-dependent simulation.

The velocity profile after the formation of the MHD pedestal is shown in Fig. 8. The figure shows the poloidal velocity (red curve, circles) and the poloidal Mach number (blue curve) versus the major radius of the plasma along the midplane. The shape of the velocity source (S_{mom}/ρ) is also shown for reference in arbitrary units (dashed grey line). Since the source is defined following Eq. (9), its strength on the midplane is nonzero only in the outboard part of the plasma. Several points can be made from Fig. 8. First, the velocity shape and the source shape are quite dissimilar: The source is smooth in space, while the velocity has a sharp gradient near the region where the poloidal Mach number crosses unity (transonic discontinuity). Not surprisingly, the velocity profile is well aligned with the source in the region where M_p is small. That is because no plasma properties (density, pressure, etc.) are dramatically modified going from a static to a sub-slow equilibrium, and no qualitative transitions are present. Thus, in the part of the plasma that is rotating at velocities well below C_{sp}, any input velocity profile can be assigned (via the source) and obtained in the plasma. The velocity profile in the inboard part of the plasma is smooth and does not show any jump at the location where $M_p = 1$. Also, the velocity on the inboard side is larger than

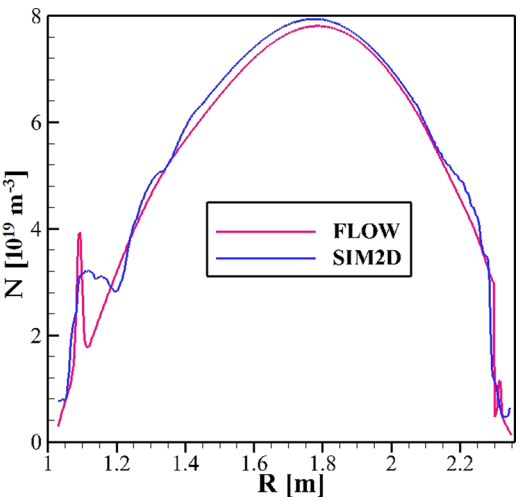

FIG. 6. (Color online) Comparison between a transonic equilibrium calculated with FLOW (red) and SIM2D quasi-steady state (blue) at time $t = 2.1\tau_p$. Density plots on the midplane are shown vs. R.

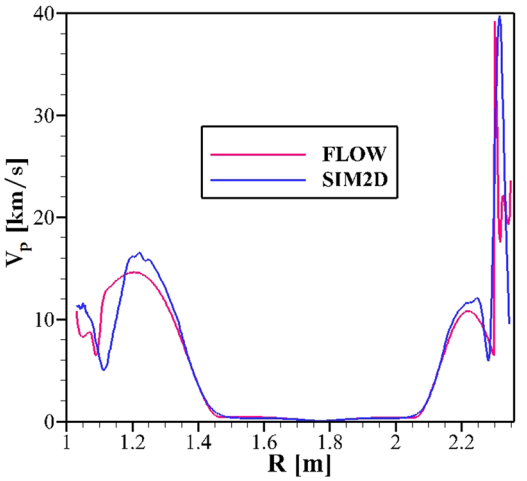

FIG. 7. (Color online) Comparison between a transonic equilibrium calculated with FLOW (red) and SIM2D quasi-steady state (blue) at time $t = 2.1\tau_p$. Poloidal velocity plots on the midplane are shown vs. R.

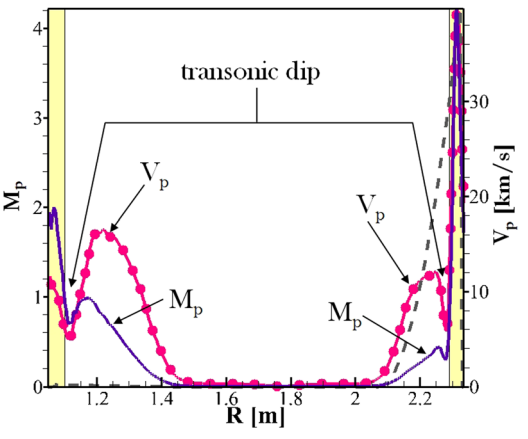

FIG. 8. (Color online) Poloidal velocity (red, circles) and poloidal Mach number (blue, solid line) on the midplane at time $t = 2.5\tau_p$. Only the main plasma region is shown. The velocity source (in [a.u.]) is also shown for reference with a grey, dashed line.

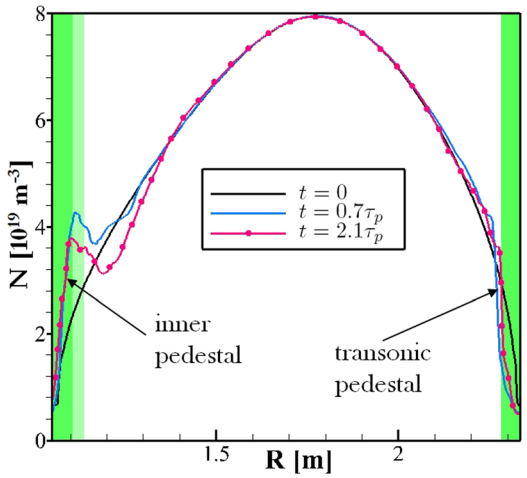

FIG. 9. (Color online) Plasma density at time $t=0$ (black), at time $t=0.7\tau_p$ (blue, solid line), at time $t=2.1\tau_p$ (red, circles). The shaded area corresponds to supersonic flows.

the velocity on the outboard side if the flow is subsonic, while the opposite holds for supersonic flow,

$$\begin{aligned} V_p^{(inboard)} &> V_p^{(outboard)} \qquad \text{if } M_p < 1 \\ V_p^{(inboard)} &< V_p^{(outboard)} \qquad \text{if } M_p > 1. \end{aligned} \tag{10}$$

This is in agreement with the predictions of the theory and of equilibrium calculations.[3,18] The Mach number profile also agrees with the theoretical expectations. The profile in the outboard part of the plasma crosses the $M_p=1$ value with a sharp gradient, while the profile in the inboard part of the plasma crosses $M_p=1$ smoothly. One interesting property of transonic equilibria and of the results of SIM2D simulations is the presence in the velocity profile of a minimum just before the MHD pedestal. The minimum, which we call the "transonic dip," is highlighted in Fig. 8.

Figure 9 shows density profiles at times $t=0.7\tau_p$ (blue line, shortly after the shock formation, but after the shock has moved away from the midplane), and at time $t=2.1\tau_p$ (red line, circles). Profiles are plotted on the midplane versus the major radius. The steepening of the density profile with respect to the initial one after the shock formation is visible in both curves at $t>0$. In particular, the profile steepens in the outboard part of the plasma, where the formation of the transonic pedestal is expected. The inner pedestal, due to the mass redistribution along the poloidal angle during the transient, is also visible. Figure 9 emphasizes that the transonic pedestal forms because the density in the supersonic region is *reduced* with respect to the initial density, while the inner pedestal is generated by a density *increase* in the supersonic region. The supersonic region is shaded in Fig. 9. The position of the $M_p=1$ surface does not change from $t=0.7\tau_p$ to $t=2.1\tau_p$ in the outboard part of the plasma, but it moves inward (to larger R) in the inner region. The area shaded with a different color is supersonic at $t=0.7\tau_p$ and subsonic at $t=2.1\tau_p$. At both times the inner pedestal is entirely located in the supersonic region. One additional point that can be recognized in Fig. 9 is that the density profile actually steepens in time. This strengthens the point that the MHD pedestal is not created by the shock. Rather, the shock forces the velocity profile to adjust so that there are no plasma regions flowing in the prohibited Mach number range. The quasi-steady state discontinuous velocity profile makes the density relax to a profile that is also discontinuous. Clearly it would not be reasonable for the density gradient to keep steepening in time if the initial steepening was created by the shock. Even at later times in the simulation the transonic pedestal retains its steep profile: The outer pedestal region at time $t=4\tau_p$ extends over about four (out of 500) grid points. Even though an exact steady state cannot be reached, the robustness of the MHD pedestal confirms the understanding that discontinuous profiles are indeed a natural equilibrium solution for MHD systems in the presence of transonic poloidal flow.

One final point that is worth mentioning is that the main modifications with respect to the initial profiles are observed in density and velocity. Since pressure is low near the transonic surface, no dramatic modification of the pressure profile is observed in our simulations. Temperature, and therefore sound speed, is not affected by the transient. Also, since β is small in the region interested by the transient, no appreciable modifications are predicted for any of the components of the magnetic field. This also leaves the poloidal sound speed (and the poloidal magneto-slow speed) essentially unchanged throughout the transient.

V. DISCUSSION

After discussing the formation of the MHD pedestal, it is worthwhile to address the issue of its relevance to experimental results. A definite conclusion on whether the formation of the MHD pedestal is involved in the L-H transition cannot be reached with the experimental data available to date. In addition, a kinetic theory needs to be developed to confirm the validity of this theory in the long mean free path regime. There are several hints that seem to indicate a plausible correlation between the predictions of the model here described and the findings of experiments.

For completeness, we first consider a point where the MHD pedestal model is not sufficient to reproduce experimental properties, namely the physics of pedestal height and width, which are governed by 3-D MHD considerations. In particular, the pedestal height is determined by the stability of peeling-ballooning modes,[19] and cannot be directly reproduced by 2D MHD simulations. The stability limit, however, refers to the pressure, rather than the density, pedestal. Since the initial temperature and pressure pedestals are small in the MHD pedestal model, it is reasonable to expect an initial pressure pedestal below the peeling-ballooning stability limit, allowing for a direct comparison between calculated and experimental density pedestal profiles just after the L-H transition. It is our conjecture that the transonic velocity discontinuity causes an edge transport barrier. This will lead to a steepening of the pedestal temperature not included in current MHD simulations. It is only at later times that the temperature and pressure buildup would bring the pedestal to the peeling-ballooning stability limit.

We next consider the range of velocities that are necessary to create the transonic discontinuity. As shown in the

previous section and in equilibrium calculations,[16] the poloidal velocities required by the model are not unreasonable when compared to experimental measurements. Indeed, velocities of the order of tens of kilometers per second are observed in experiment, either via impurity or main ion measurements.[20–22] It is pointed out that the steady-state velocities shown in the present paper (e.g., in Fig. 8) do not correspond to the minimum velocities required to obtain transonic discontinuities. In principle, velocities just above the poloidal magneto-slow speed are sufficient to create transonic discontinuities, and it is not necessary to have the Mach numbers as high as $M_p \simeq 3-4$ shown in Fig. 8.

One possible concern about equilibria with high poloidal velocity is the power dissipation that occurs in the pedestal region due to poloidal viscosity. It is straightforward to evaluate the ratio f_{rot} between the power dissipated due to poloidal rotation and the total plasma power exhaust. This is done in Eq. (11), where quantities denoted with C are calculated in the core of the plasma, quantities denoted with S are calculated in the supersonic flow region at the foot of the pedestal, and all symbols have their usual meaning (ν_{ii} is the ion-ion collision frequency, r_L is the Larmor radius, is the inverse aspect ratio, q is the safety factor and n the plasma number density),

$$f_{rot} = \frac{\int_{supersonic} \nu_{ii}\rho V_p^2 d\mathbf{r}}{\left(\int_{plasma} \frac{3}{2} p d\mathbf{r}\right)\Big/ \tau_E} = \frac{4}{3}\nu_{ii}^C \tau_E \left(\frac{n_S}{n_{core}}\right)^2 \left(\frac{\Delta_S}{r_{L\theta}^S}\right) \frac{r_L^C}{a} \left(\frac{M_p}{3}\right)^2 \frac{9\epsilon}{q_S}, \quad (11)$$

where Δ_S is the width of the supersonic flow region at the foot of the pedestal. We assume that the width of the supersonic region is of the order of the poloidal Larmor radius, and use a set of characteristic values $\epsilon^{-1} \simeq q_S \simeq M_p \simeq 3$, leading to

$$f_{rot} \simeq \frac{4}{3}\nu_{ii}^C \tau_E \left(\frac{n_S}{n_{core}}\right)^2 \rho_C^*, \quad (12)$$

where ρ^* is the normalized Larmor radius. Direct evaluation of Eq. (12) with reasonable DIII-D parameters (namely, $n_{core} = 10 n_S$, $T_{core} = 3keV$, $B = 1.3T$, $\tau_E = 0.3s$) gives $f_{rot} \simeq 2\%$. Different assumptions for the plasma properties give slightly different numerical values, but f_{rot} is in general much smaller than unity. This shows that radial transport can easily remove the viscous heating dissipated by the poloidal flow.

Still regarding a possible comparison with experimental measurements, we calculated the normal (to magnetic surfaces) component of the electric field, taking into account plasma velocity and resistivity. The field is plotted on the midplane versus the major radius in Fig. 10. At this location, the unit vectors $\hat{e}_\psi$ and $\hat{e}_r$ are aligned, and the results of our calculations can be directly compared to the radial electric field inferred from impurity velocity measurements. Looking for instance at Fig. 3 of Ref. 22 or Fig. 4 of Ref. 20, it is seen

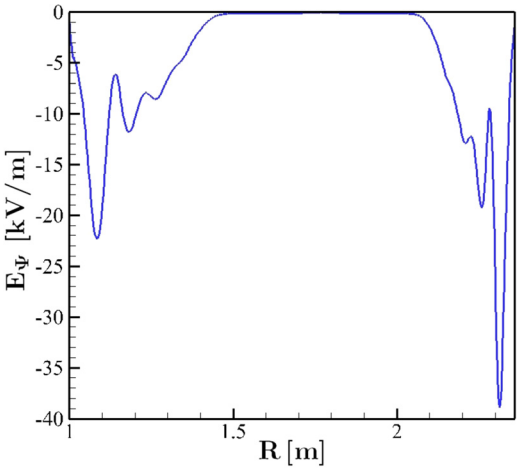

FIG. 10. (Color online) Normal electric field along the midplane at time $t = 1.2\tau_p$ due to poloidal flow.

that the electric field obtained from SIM2D simulations at the location of the pedestal ($\sim$40 kV/m) is in the same range of the field measured near the edge in H-mode plasmas.

Several additional qualitative hints on the relevance of the MHD pedestal model to the L-H transition can be found in experiments. The rationale behind all of them is in the fact that lowering the poloidal sound speed (which we again use to approximate the poloidal magneto-slow speed) will also lower the poloidal velocity necessary to create the MHD pedestal. Therefore, if the proposed model is correct, any modification to the experimental setup that will lower the poloidal sound speed should make the L-H transition easier, i.e., lower the power threshold for the transition (since we are assuming that the flow drive is related to the input power). For instance, configurations with X-points should have lower power threshold, because the poloidal sound speed vanishes at the X-point (where $B_p = 0$). This is indeed observed in experiments. Moreover, the power threshold should be even lower in configurations with two X-points, where the poloidal sound speed vanishes in two points. The argument holds for "true" double null configurations, where the two X-points are located on the same magnetic surface. Experimental findings seem to indicate that the presence of two X-points on the same magnetic surface does facilitate the L-H transition.[23] Another way to lower the poloidal sound speed is to increase the mass of the main ion species, since the sound speed scales like $\sqrt{1/m_i}$. The arguments hold of course only if the plasma temperature remains the same. Once again, experiments indicate the power threshold is lower for deuterium than for hydrogen.[24] This is in fact common wisdom, even though exceptions are found in some experiments. Finally, the poloidal sound speed can be decreased by lowering the edge temperature. This can be accomplished for instance by puffing gas at the plasma edge. Experiments indicate that this is the case,[25] providing one more indirect confirmation of the relevance of transonic discontinuities to the L-H transition.

One additional point that deserves at least a brief discussion is the origin on the momentum source. As mentioned earlier, the origin of the momentum source is not essential for the formation of the MHD pedestal. Several mechanisms for poloidal momentum generation have been proposed in

the literature to drive poloidal flows to a velocity well above the neoclassical value.[26–30] Perhaps the most intuitive mechanism is due to non-ambipolar losses at the edge.[31] An excess of ion losses with respect to electron losses, e.g., due to fast-ion losses, creates a radial electric field near the plasma edge, which drives an $\underline{E} \times \underline{B}$ flow in the poloidal direction. It as also been known for a long time that anomalous transport can cause the plasma to start rotating without any external momentum source.[32] Yet another possibility is for turbulent transport to create a source for poloidal rotation.[33,34]

Based on the large number of possibilities for driving poloidal flows, and on the experimental observation of poloidal velocities not far from the ones obtained in our simulations, it seems possible that a positive correlation between transonic equilibria and L-H transition can be found with a detailed analysis of experimental results. Incidentally, this is not a trivial issue, since very detailed (in space and time) measurements of density, temperature, and poloidal velocity during the L-H transition are needed to ascertain whether this correlation does in fact exist. A feature of the MHD pedestal is the "transonic dip," i.e., the minimum in the poloidal velocity radial profile just before the pedestal (Figs. 7 and 8). Measurements of such a minimum could be a strong confirmation of the transonic character of the pedestal formation.

In conclusion, the MHD pedestal model has several attractive properties that seem to indicate a relation with the L-H transition. The simulations presented in this paper show that, at least within the limit of the resistive MHD model, the discontinuous transonic equilibrium is a natural state for the plasma, dynamically accessible if poloidal rotation is present in the system.

ACKNOWLEDGMENTS

This work was supported by DOE under Grant No. DE-FG02-93ER54215.

[1]J. D. Lawson, Proc. Phys. Soc. London Sect. B **70**, 6 (1957).
[2]F. Wagner, G. Becker, K. Behringer, D. Campbell, A. Eberhagen, W. Engelhardt, G. Fussmann, O. Gehre, J. Gernhardt, G. v. Gierke, G. Haas, M. Huang, F. Karger, M. Keilhacker, O. Klüber, M. Kornherr, K. Lackner, G. Lisitano, G. G. Lister, H. M. Mayer, D. Meisel, E. R. Müller, H. Murmann, H. Niedermeyer, W. Poschenrieder, H. Rapp, H. Röhr, F. Schneider, G. Siller, E. Speth, A. Stäbler, K. H. Steuer, G. Venus, O. Vollmer, and Z. Yü, Phys. Rev. Lett. **49**, 1408 (1982).
[3]R. Betti and J. P. Freidberg, Phys. Plasmas **7**, 2439 (2000).
[4]L. Guazzotto, R. Betti, J. Manickam, and S. Kaye, Phys. Plasmas **11**, 604 (2004).
[5]A. J. C. Beliën, M. A. Botchev, J. P. Goedbloed, B. van der Holst, and R. Keppens, J. Comput. Phys. **182**, 91 (2002).
[6]J. P. Goedbloed, Phys. Scr. T **98**, 43 (2002).
[7]J. P. Goedbloed, A. J. C. Beliën, B. van der Holst, and R. Keppens, Phys. Plasmas **11**, 28 (2004).
[8]L. Guazzotto and R. Betti, Phys. Rev. Lett. **107**, 125002 (2011).
[9]H. Biglari, P. H. Diamond, and P. W. Terry, Phys. Fluids B **2**, 1 (1990).
[10]E. Hameiri, Phys. Fluids **26**, 230 (1983).
[11]A. Jeffrey and T. Taniuti, *Non-Linear Wave Propagation: With Applications to Physics and Magnetohydrodynamics* (Academic, 1964).
[12]J. P. H. Goedbloed and S. Poedts, *Principles of Magnetohydrodynamics: With Applications to Laboratory and Astrophysical Plasmas* (Cambridge University Press, 2004).
[13]K. G. McClements and M. J. Hole, Phys. Plasmas **17**, 082509 (2010).
[14]R. W. MacCormack, AIAA Paper **69**, 354 (1969).
[15]J. U. Brackbill and D. C. Barnes, J. Comput. Phys. **35**, 462 (1980).
[16]L. Guazzotto and R. Betti, Phys. Plasmas **12**, 056107 (2005).
[17]A. B. Hassam, Nucl. Fusion **36**, 707 (1996).
[18]R. F. Schmitt, L. Guazzotto, H. Strauss, G. Y. Park, and C.-S. Chang, Phys. Plasmas **18**, 022502 (2011).
[19]P. B. Snyder, N. Aiba, M. Beurskens, R. J. Groebner, L. D. Horton, A. E. Hubbard, J. W. Hughes, G. T. A. Huysmans, Y. Kamada, A. Kirk, C. Konz, A. W. Leonard, J. Lonnroth, C. F. Maggi, R. Maingi, T. H. Osborne, N. Oyama, A. Pankin, S. Saarelma, G. Saibene, J. L. Terry, H. Urano, and H. R. Wilson, Nucl. Fusion **49**, 085035 (2009).
[20]J. Kim, K. H. Burrell, P. Gohil, R. J. Groebner, Y.-B. Kim, H. E. St. John, R. P. Seraydarian, and M. R. Wade, Phys. Rev. Lett. **72**, 2199 (1994).
[21]K. D. Marr, B. Lipschultz, P. J. Catto, R. M. McDermott, M. L. Reinke, and A. N. Simakov, Plasma Phys. Controlled Fusion **52**, 055010 (2010).
[22]R. M. McDermott, B. Lipschultz, J. W. Hughes, P. J. Catto, A. E. Hubbard, I. H. Hutchinson, R. S. Granetz, M. Greenwald, B. LaBombard, K. Marr, M. L. Reinke, J. E. Rice, D. Whyte, and Alcator C-Mod Team, Phys. Plasmas **16**, 056103 (2009).
[23]H. Meyer, P. G. Carolan, G. D. Conway, G. Cunningham, L. D. Horton, A. Kirk, R. Maingi, F. Ryter, S. Saarelma, J. Schirmer, W. Suttrop, H. R. Wilson, the MAST, A. Upgrade, and N. teams, Nucl. Fusion **46**, 64 (2006).
[24]P. Gohil, T. C. Jernigan, J. T. Scoville, and E. J. Strait, Nucl. Fusion **49**, 115004 (2009).
[25]J. A. Snipes *et al.*, *Proceedings of the 19th International Conference on Fusion Energy*, CT/P04 (Lyon, France 2002).
[26]M. N. Rosenbluth and F. L. Hinton, Phys. Rev. Lett. **80**, 724 (1998).
[27]G. Kagan, K. D. Marr, P. J. Catto, M. Landreman, B. Lipschultz, and R. McDermott, Plasma Phys. Controlled Fusion **53**, 025008 (2011).
[28]W. M. Stacey, Phys. Plasmas **9**, 3874 (2002).
[29]I. Pusztai and P. J. Catto, Plasma Phys. Controlled Fusion **52**, 075016 (2010).
[30]H. A. Claassen, H. Gerhauser, A. Rogister, and C. Yarim, Phys. Plasmas **7**, 3699 (2000).
[31]K. C. Shaing and E. C. Crume, Phys. Rev. Lett. **63**, 2369 (1989).
[32]T. E. Stringer, Phys. Rev. Lett. **22**, 770 (1969).
[33]W. J. T. Bos, S. Neffaa, and K. Schneider, Phys. Rev. Lett. **101**, 235003 (2008).
[34]H. J. H. Clercx, S. R. Maassen, and G. J. F. van Heijst, Phys. Rev. Lett. **80**, 5129 (1998).